Weibull Analysis of Dielectric Breakdown in a Self-Assembled Nanodielectric for Organic Transistors

ARTICLE *in* JOURNAL OF PHYSICAL CHEMISTRY LETTERS · NOVEMBER 2010

Impact Factor: 7.46 · DOI: 10.1021/jz101325r

7 AUTHORS, INCLUDING:

Kunho Yoon
Northwestern University
4 PUBLICATIONS **73** CITATIONS
SEE PROFILE

Lisa A Fredin
National Institute of Standards and Technol…
11 PUBLICATIONS **161** CITATIONS
SEE PROFILE

Mark A. Ratner
Northwestern University
906 PUBLICATIONS **42,483** CITATIONS
SEE PROFILE

Lincoln J Lauhon
Northwestern University
182 PUBLICATIONS **10,638** CITATIONS
SEE PROFILE

THE JOURNAL OF PHYSICAL CHEMISTRY Letters

pubs.acs.org/JPCL

Weibull Analysis of Dielectric Breakdown in a Self-Assembled Nanodielectric for Organic Transistors

Ruth A. Schlitz,[†,§] KunHo Yoon,[†,§] Lisa A. Fredin,[‡,§] Young-geun Ha,[‡,§] Mark A. Ratner,[*,†,‡,§] Tobin J. Marks,[*,†,‡,§] and Lincoln J. Lauhon[*,†,§]

[†]Department of Materials Science and Engineering, Northwestern University, 2220 Campus Drive, Evanston, Illinois 60208, United States, [‡]Department of Chemistry, Northwestern University, 2145 Sheridan Rd., Evanston, Illinois 60208, United States, and [§]Materials Research Science and Engineering Center, Northwestern University, 2145 Sheridan Rd., Evanston, Illinois 60208, United States

ABSTRACT The effect of thermal annealing on leakage current and dielectric breakdown in self-assembled nanodielectric (SAND) metal−insulator−semiconductor (MIS) devices is investigated. Annealing at temperatures of ≥300 °C for 120 s in a reducing atmosphere significantly reduces the leakage current density at typical operating voltages (V_g = 3 V) while greatly narrowing the distribution of breakdown voltages. The threshold breakdown voltage is characterized by a Weibull distribution of slope $\beta \approx 4.5$ prior to thermal annealing, and by $\beta \geq 12$ post annealing. A comparison of the breakdown characteristics of conventional inorganic dielectrics with those of SAND demonstrates that self-assembly is a viable approach to fabricating highly reliable dielectric materials for unconventional electronics.

SECTION Electron Transport, Optical and Electronic Devices, Hard Matter

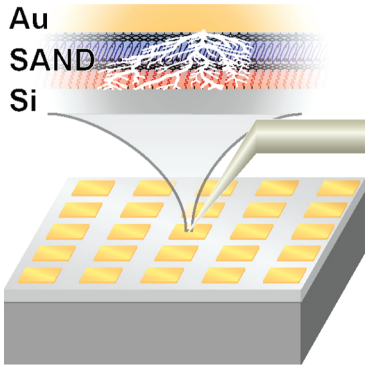

The performance of many devices fabricated with unconventional semiconductors can be significantly enhanced by using self-assembled monolayers and multilayers as gate dielectrics.[1,2] For this purpose, self-assembled nanodielectrics (SANDs) have a particularly compelling combination of properties, including a sizable dielectric constant (k as high as 16),[3] low leakage current densities ($J_{leak} = 10^{-7} - 10^{-8}$ A/cm^2 at 1 V bias),[3,4] and a low density of pinhole defects. Furthermore, SANDs are robust to both thermal[5] and ionizing[6] radiation, are solution processable,[3] optically transparent,[7−9] mechanically flexible,[7,9] and exhibit a low interface state density in contact with a remarkably wide range of materials.[3,5,10−13] The low interface state density in particular makes a SAND an appealing dielectric for nanomaterials grown from the "bottom up" as has been demonstrated in a variety of proof-of-principle devices.[7,9,14,15] For these reasons, statistical studies of the fundamental electrical properties of large numbers of devices are important to understanding the intrinsic characteristics of a SAND that will predict performance in a wide range of applications.

Prior investigations of SAND electronic transport in regimes of moderate bias have revealed low-field transport mechanisms,[4] but the range of voltages that cause irreversible dielectric breakdown has not yet been studied systematically. A statistical analysis of the stable operating regime for devices incorporating SAND would therefore be desirable. It is also important to characterize how the dielectric properties change after exposure to elevated temperatures, since devices such as organic transistors are often annealed at various stages in the processing in order to, for example, improve crystallinity of a solution-deposited channel material or reduce contact resistance. Importantly, thermal annealing is known to reduce SAND leakage current densities and to increase the capacitance, possibly resulting from condensation of "dangling" SiOH groups at higher temperatures.[5] One might therefore expect that annealing would have a favorable impact on the dielectric breakdown voltage as well.

Here we report measurement and statistical analysis of the threshold voltage for irreversible dielectric breakdown in SAND metal−insulator−semiconductor (MIS) devices, both before and after thermal annealing, using Weibull analysis.[16] It will be seen that the distribution of breakdown voltages is well-described by a two-parameter Weibull distribution[17] with a Weibull slope comparable to that of conventional inorganic dielectrics having a similar thickness [$\beta \approx 3-6$ for 5.5-nm SiO_2],[18−20] and that thermal annealing dramatically improves the uniformity of the breakdown distribution. The physical parameters and processes associated with SAND dielectric breakdown are considered in the context of the Weibull analysis.

Initial annealing studies were performed on 60 × 60 μm^2 area MIS devices consisting of an n^{++} Si substrate, three layers of type III SAND,[1−3] and Ti/Au (30 nm/60 nm) contacts deposited using a shadow mask and e-beam evaporation. Type III SAND, shown in Figure 1a, consists of a charge-blocking alkyl layer (Alk), a highly polarizable π-electron stilbazolium layer (Stb), and a highly cross-linked siloxane capping layer

Received Date: September 23, 2010
Accepted Date: October 27, 2010
Published on Web Date: November 04, 2010

DOI: 10.1021/jz101325r | J. Phys. Chem. Lett. 2010, 1, 3292–3297

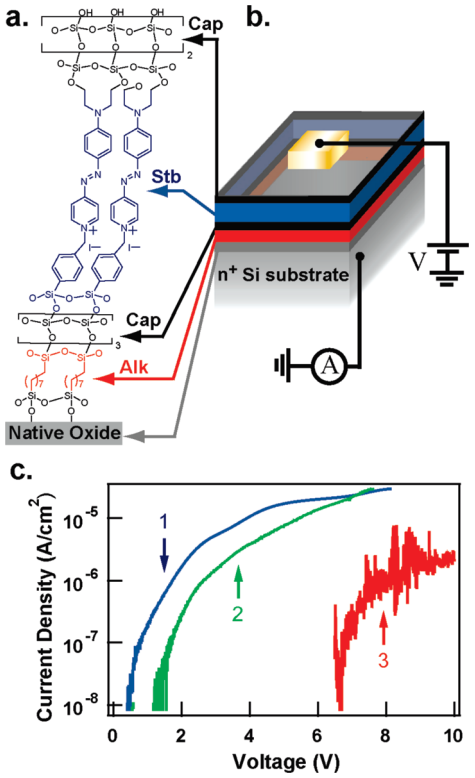

Figure 1. Measurement of J_{leak} for SAND MIS devices. (a) Structure of type III SAND, showing the alkyl charge-blocking layer (Alk), the polarizable stilbazolium layer (Stb), and the siloxane capping layer (Cap). (b) Schematic of a SAND MIS device and measurement geometry, showing the voltage applied to an Au contact. (c) Representative $J_{leak}-V$ curves for 60×60 μm^2 MIS devices with three SAND layers: Sample **1** (unannealed, blue); Sample **2** (annealed before contact deposition, green), and Sample **3** (contacted and then annealed, red).

(Cap). The type III SAND employed here was assembled using the published procedure with minor modifications, and each trilayer is 5.5 nm thick.[3] Devices are typically fabricated using three layers of type III SAND (16.5 nm total thickness) to reduce leakage currents while retaining an acceptable capacitance.[5−15,21] In the present work, current−voltage ($I_{leak}-V_g$) curves were measured for each device and normalized by the device area; a schematic is shown in Figure 1b. Devices measured prior to thermal annealing are referred to as Sample **1**. Sample **3** refers to devices annealed at 350 °C for 120 s in forming gas (95% N_2, 5% H_2) to discourage Ti oxidation. Additional devices were fabricated for which the SAND layer was annealed prior to contact metal deposition (Sample **2**).

In annealing experiments with three layers of type III SAND, it is found that annealing devices greatly reduces the leakage current density (J_{leak}) at 3 V bias from 5.4×10^{-6} A/cm^2 (Sample **1**) to below the preamplifier detection limit of about 5 pA, which for these samples is about 1.4×10^{-7} A/cm^2 (Sample **3**). Indeed, the J_{leak} of Sample **3** became detectable only at >6 V bias. Interestingly, Sample **2** (pre-annealed SAND) also showed reduced leakage current density, but the reduction is smaller in magnitude (9.1×10^{-7} A/cm^2 at 3 V bias). Annealing also produces notable qualitative changes

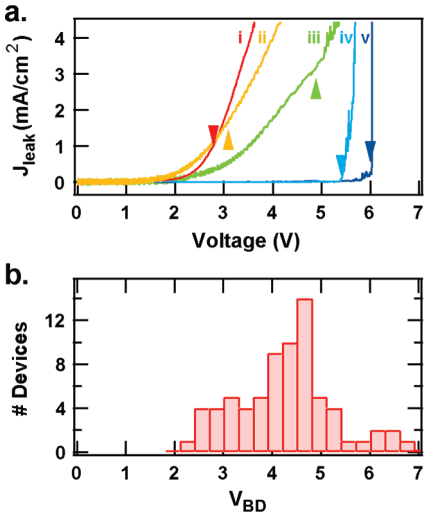

Figure 2. Weibull analysis of breakdown voltage in MIS devices with one SAND layer. (a) Representative $J_{leak}-V_g$ plots for five distinct devices on Sample **6** (200×200 μm^2), labeled i−v. The triangles indicate the V_{BD} extracted for each curve. (b) Histogram of extracted V_{BD}. The bin size is 0.3 V.

in the $J_{leak}-V_g$ characteristics. While Sample **2** (preannealed SAND), exhibits a gradual increase in current similar to Sample **1** (unannealed), Sample **3** devices (annealed device) exhibit no detectable current until a sudden onset at higher bias (Figure 1c). The reduction in leakage current density and detectable current onset may reflect silanol condensation at higher temperatures as noted above.[5] From studies of many devices, it was confirmed that the presence of the contacts enhances the reduction in leakage current density caused by annealing, perhaps by protecting the SAND from background gases in the annealer. Alternatively, contact−SAND interactions or oxidation of the Ti layer into insulating TiO_2 may contribute to the reduced current density.

To exclude the possibility of Ti oxidation and to isolate the intrinsic behavior of SAND with annealing, extensive studies were performed on 100×100 μm^2 area and 200×200 μm^2 area Au-contacted n^{++} Si substrate/1 layer SAND/50 nm Au MIS devices. The Au was deposited by thermal evaporation to minimize SAND exposure to ionizing radiation and particulates possibly present during e-beam evaporation.[4] Devices were then annealed at 300 °C in forming gas for 120 s. $I_{leak}-V$ data were acquired for at least 50 devices of each sample. $J_{leak}-V_g$ curves from the 200×200 μm^2 devices reveal a range of breakdown voltages (Figure 2a). Annealing reduces the average leakage current density of these one-layer Au-contacted devices by 3−4 times at $V_g = 3$ V (Table 1); because no Ti was present in these devices, we can rule out Ti oxides as the cause of the reduced leakage current. Au-contacted devices were therefore used to investigate SAND dielectric breakdown characteristics before and after annealing.

We defined breakdown voltage (V_{BD}) as the voltage at which the device exhibits a differential conductance, dI_{leak}/dV_g, exceeding 10^{-6} S. This threshold value was chosen because it is (1) readily detectable by an automated algorithm and (2) the extracted Weibull parameters were relatively insensitive to the exact slope in this conductance range. The differential

DOI: 10.1021/jz101325r | J. Phys. Chem. Lett. 2010, 1, 3292–3297

Table 1. Average Leakage Current Density and Processing of Type III SAND at $V_g = 3$ V Bias

sample #	# SAND layers	contact metal	anneal temp.[a]	capacitor area (cm^2)	J_{leak} at 3 V bias ($\mu A/cm^2$)
1	3	Ti/Au		3.6×10^{-5}	5.4 ± 3.2
2	3	Ti/Au	350 °C[b]	3.6×10^{-5}	0.91 ± 0.51
3	3	Ti/Au	350 °C	3.6×10^{-5}	[c] < 0.19
4	1	Au		1.0×10^{-4}	54 ± 33
5	1	Au	300 °C	1.0×10^{-4}	16 ± 11
6	1	Au		4.0×10^{-4}	520 ± 180
7	1	Au	300 °C	4.0×10^{-4}	130 ± 88

[a] All samples annealed for 120 s in 95% N 5% H. [b] SAND annealed prior to contact deposition. [c] Below detection limit of preamplifier (~5 pA).

conductance was determined by fitting a line to the $I_{leak}-V_g$ data over a range of 0.1 V. V_{BD} values extracted numerically by this algorithm are indicated by arrows on the representative $J_{leak}-V_g$ curves in Figure 2a. Histograms of V_{BD} for $200\times200\ \mu m^2$ and $100\times100\ \mu m^2$ devices are shown in Figures 2b and 4a, respectively. Inspection of the V_{BD} histograms suggests that the V_{BD} distribution has a single distinct peak. The distribution of breakdown voltages was next fit to the Weibull distribution, a statistical description of weakest link behavior.[22] For example, if a single defect or pinhole exists in the dielectric, the device may exhibit a significant leakage current.[23−27] The Weibull cumulative distribution function, F, is defined as

$$F(V_{BD}) = 1 - \exp\left[-\left(\frac{V_{BD}}{\alpha}\right)^{\beta}\right]$$

where α, the scale parameter, is the voltage at which 63% of the capacitors have broken down, and β, the shape parameter, is the Weibull modulus indicating the width of the distribution. The Weibull cumulative distribution function is typically rearranged by taking two logarithms,

$$\ln[-\ln(1-F)] = \beta \ln(V_{BD}) - \beta \ln \alpha$$

so that the slope, β, and the y-intercept, $-\beta \ln \alpha$, are readily extracted from a plot of $\ln[-\ln(1-F)]$ versus $\ln(V_{BD})$; data that conform to the Weibull distribution will fall along a line (Figure 3). Linear regression was used to determine α and β for Samples **4** and **6**, as tabulated in Table 2.

Fitting to the Weibull distribution assumes that breakdown occurs at locations that are distributed randomly throughout the self-assembled multilayer according to a Poisson distribution, as would be the case for randomly distributed defects. If the breakdown sites are in fact randomly distributed, the V_{BD} values of capacitors with differing areas will follow the scaling law:[23]

$$\frac{V_{BD1}}{V_{BD2}} = \left[\frac{A_2}{A_1}\right]^{1/\beta}$$

Thus the V_{BD1} data will form a line parallel to that of the V_{BD2} data on a Weibull plot, and the lines will overlap if scaled by $\ln(A_2/A_1)$. The inset to Figure 3 compares the $200\times200\ \mu m^2$ data (Sample **6**) with scaled $100\times100\ \mu m^2$ data (Sample **4**), indicating that the data follow the expected scaling law.

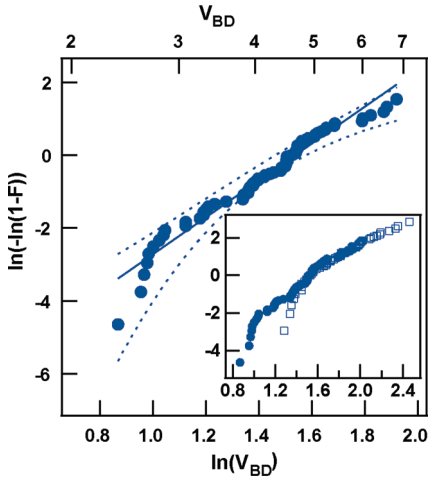

Figure 3. Weibull plot for Sample **6** . The dashed lines represent 95% confidence bounds, and the solid line is the fit to the data. (inset) Area-normalized (offset) Weibull plot for Sample **4** ($100\times100\ \mu m^2$ − open squares) normalized to the area of Sample **6** (filled circles), confirming area scaling.

Furthermore, if the scaling law applies, the β will be indistinguishable for devices of A_1 and A_2; this is the case for Samples **4** and **6**, as the confidence bounds on β overlap (Table 2).

Inspection of the transformed data in Figure 3 shows deviations from the Weibull distribution for low V_{BD}, low probability events. This tail, consisting of less than 10% of the data, might indicate (1) the existence of a distinct mechanism dominating low-voltage breakdown, (2) the existence of a threshold voltage beneath which SAND does not undergo breakdown,[22] or (3) the presence of a significant underlying variability in a device parameter. The presence of a threshold voltage can be tested by a three-parameter Weibull cumulative probability distribution of the form

$$F(V_{BD}) = 1 - \exp\left[-\left(\frac{V_{BD}-\delta}{\alpha}\right)^{\beta}\right]$$

where δ is a threshold voltage below which the probability of dielectric breakdown is zero.[22] If, for example, breakdown in the SAND occurs only above a critical electric field or electron energy, this will manifest as a common δ for both the $100\times100\ \mu m^2$ and $200\times200\ \mu m^2$ devices.[22] Linear regression of the three-parameter distribution gives $\delta_{100} = 3.5$ ($3.1 < \delta_{100} < 3.6$)

DOI: 10.1021/jz101325r | J. Phys. Chem. Lett. 2010, 1, 3292–3297

Table 2. Weibull Parameters for One Layer of Type III SAND

sample #	n	scale parameter α (V), 95% confidence range	shape parameter β, 95% confidence range	r^2
4	53	7.0 [6.5 < α < 7.5]	4.0 [3.3 < β < 4.9]	0.91
5[a]	72	4.39 [4.35 < α < 4.42]	37 [29 < β < 46]	0.97
6	63	4.7 [4.4 < α < 4.9]	5.1 [4.4 < β < 4.6]	0.96
7[a]	61	4.2 [4.1 < α < 4.3]	12 [9.7 < β < 15]	0.92

[a] With data excluded as described in the text and Figure 4.

V and δ_{200} = 1.9 (1.6 < δ_{200} < 2.2) V. The present data do not therefore support the existence of a common *minimum* breakdown voltage between the two samples. Note, however, that the criterion for defining the breakdown voltage should be refined before the existence of a minimum threshold is discounted; the qualitative variations in the rate of slope increase in Figure 2a may result in the premature report of irreversible breakdown, i.e., it is possible that all breakdown below a certain voltage is reversible. Further investigations are needed to address this issue.

Returning to the deviations from a single Weibull slope, underlying variations in SAND thickness or packing density are possible contributing factors. For instance, the root-mean-square (rms) roughness of one-layer type III SAND has been reported to be 0.5−1 nm;[3] given the 5.5 nm thickness, these variations might lead to significantly differing path lengths for electronic transport through SAND. Thickness variations in ultrathin silicon oxides have previously been modeled by the q-Weibull distribution, which also has three parameters.[28−30] In the present study, fitting the data to the q-Weibull distribution did not significantly improve r^2 versus the two-parameter distribution, so underlying variability is neither confirmed nor ruled out. We conclude that the breakdown threshold in the majority of SAND MIS devices is dominated by a single mechanism, although the two-parameter fit *overestimates* failure at low voltages.

Upon annealing samples **4** and **6** to produce samples **5** and **7**, respectively, the distribution of breakdown voltages narrows significantly (Figure 4a). Although the Weibull plots in Figures 4b,c reveal an increase in slope upon annealing, in each case there is also a low-probability, high V_{BD} tail containing less than 10% of the data that is not well fit by the Weibull slope of the remaining data. Intriguingly, the high-voltage tail appears to have a slope similar to that of the unannealed distribution. This observation leads us to consider two hypotheses. First, devices that survive to higher voltages may undergo dielectric breakdown by a different mechanism. A larger data set is recommended to further establish the presence of multiple breakdown mechanisms, which would lead to multiple Weibull slopes. Second, it is possible that any transformations within SAND induced by the annealing were incomplete.

Because the *lowest* voltages at which breakdown occurs are of interest for device applications, we excluded the upper tail from the Weibull fit for the parameters reported below. The excluded data are indicated by crosses in Figures 4b,c. To characterize the dominant breakdown mechanism, we also excluded the single "early" breakdown in Figure 4c. The Weibull modulus increases after annealing from 3.3 to 37

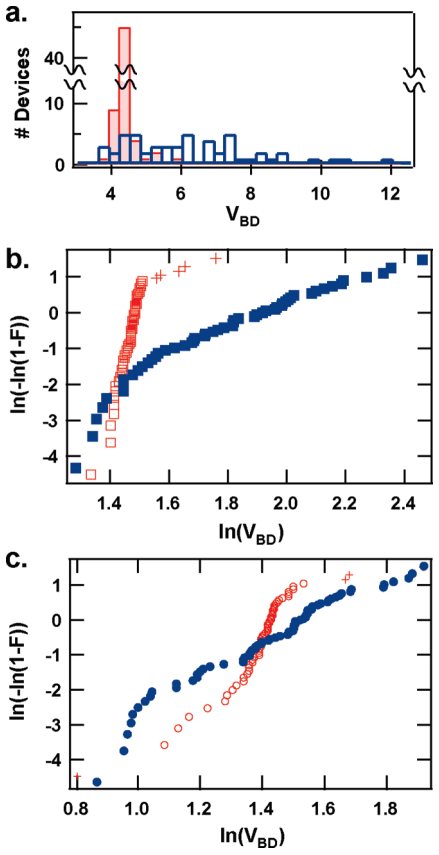

Figure 4. Distribution of V_{BD} in single layer SAND MIS devices before and after annealing. (a) Histograms of V_{BD} for 100×100 μm^2 devices before annealing (Sample **4**, blue) and after a 300 °C 120 s anneal (Sample **5**, red). The bin size is 0.3 V. (b) Weibull plot for Samples **4** (blue filled squares) and **5** (red squares). (c) Weibull plot for 200×200 μm^2 devices before annealing (Sample **6**, blue filled circles) and after a 300 °C 120 s anneal (Sample **7**, red circles).

for the 100×100 μm^2 devices and from 4.4 to 12 for the 200×200 μm^2 devices. As indicated by the error bounds on β (Table 2), area scaling is not observed for annealed samples, indicating that the defects are not randomly distributed and/or the processing conditions were not identical for the two samples. The scale parameter also changes with annealing: α decreases from 7.0 to 4.4 for 100×100 μm^2 devices and from 4.7 to 4.2 for 200×200 μm^2 devices. The data fit the Weibull distribution well, with r^2 = 0.97 and 0.92 for the 100×100 μm^2 and 200×200 μm^2 devices, respectively. The lower α indicates that the devices, as an ensemble, undergo dielectric breakdown at lower voltages despite the lower magnitudes of leakage current prior to breakdown.

DOI: 10.1021/jz101325r | J. Phys. Chem. Lett. 2010, 1, 3292–3297

Perhaps the most striking result of this investigation is that quantitative statistical analysis of SAND dielectric breakdown shows that the electrical properties of these very unconventional molecular dielectrics can be as uniform as those of conventional inorganic dielectrics, and indeed can be described by the same statistical distribution. Combining the leakage current density measurements and extracted Weibull parameters, it is also concluded that thermal processing is beneficial to SAND device reliability: not only are leakage current densities reduced at low biases, enhancing performance at typical operating voltages, but breakdown voltages are more tightly distributed, which better defines the window of operating voltages. Furthermore, since SAND is an excellent gate dielectric for a variety of channel materials that are solution-deposited and then annealed,[3,5,12,13] thermal processing provides an opportunity to improve both the channel and the SAND dielectric in a single step. In addition, annealed SAND exhibits remarkably uniform properties for a self-assembled monolayer-based material, with the distribution of breakdown voltages exhibiting a Weibull modulus of up to 37. Considering the size of our MIS devices, these results demonstrate that self-assembly is a viable approach to fabricating highly reliable defect-free dielectric materials for large-area unconventional electronics.

AUTHOR INFORMATION

Corresponding Author:

*To whom correspondence should be addressed. E-mail: ratner@chem.northwestern.edu (M.A.R.); t-marks@northwestern.edu (T.J.M.); lauhon@northwestern.edu (L.J.L.).

ACKNOWLEDGMENT We acknowledge the Northwestern University MRSEC for support of this research under NSF Grant DMR-0520513 and the ONR through contract number N00014-05-1-0766. We thank S. Renfrew for assistance in developing the Weibull analysis of SAND and K. Everaerts for discussions of SAND synthesis. R.A.S. acknowledges the support of a National Defense Science & Engineering Graduate Fellowship.

REFERENCES

(1) Ortiz, R. P.; Facchetti, A.; Marks, T. J. High-*k* Organic, Inorganic, and Hybrid Dielectrics for Low-Voltage Organic Field-Effect Transistors. *Chem. Rev.* **2010,** *110*, 205–239.

(2) DiBenedetto, S. A.; Facchetti, A.; Ratner, M. A.; Marks, T. J. Molecular Self-Assembled Monolayers and Multilayers for Organic and Unconventional Inorganic Thin-Film Transistor Applications. *Adv. Mater.* **2009,** *21*, 1407–1433.

(3) Yoon, M.; Facchetti, A.; Marks, T. J. $\sigma-\pi$ Molecular Dielectric Multilayers for Low-Voltage Organic Thin-Film Transistors. *Proc. Natl. Acad. Sci. U.S.A.* **2005,** *102*, 4678–4682.

(4) DiBenedetto, S. A.; Facchetti, A.; Ratner, M. A.; Marks, T. J. Charge Conduction and Breakdown Mechanisms in Self-Assembled Nanodielectrics. *J. Am. Chem. Soc.* **2009,** *131*, 7158–7168.

(5) Byrne, P. D.; Facchetti, A.; Marks, T. J. High-Performance Thin-Film Transistors from Solution-Processed Cadmium Selenide and a Self-Assembled Multilayer Gate Dielectric. *Adv. Mater.* **2008,** *20*, 2319–2324.

(6) Ju, S.; Lee, K.; Janes, D. B.; Dwivedi, R. C.; Baffour-Awuah, H.; Wilkins, R.; Yoon, M.; Facchetti, A.; Marks, T. J. Proton Radiation Hardness of Single-Nanowire Transistors Using Robust Organic Gate Nanodielectrics. *Appl. Phys. Lett.* **2006,** *89*, 073510/1–073510/3.

(7) Ju, S.; Facchetti, A.; Xuan, Y.; Liu, J.; Ishikawa, F.; Ye, P.; Zhou, C.; Marks, T. J.; Janes, D. B. Fabrication of Fully Transparent Nanowire Transistors for Transparent and Flexible Electronics. *Nat. Nanotechnol.* **2007,** *2*, 378–384.

(8) Ju, S.; Li, J.; Liu, J.; Chen, P.; Ha, Y.; Ishikawa, F.; Chang, H.; Zhou, C.; Facchetti, A.; Janes, D. B.; et al. Transparent Active Matrix Organic Light-Emitting Diode Displays Driven by Nanowire Transistor Circuitry. *Nano Lett.* **2008,** *8*, 997–1004.

(9) Kim, H.; Won, S. M.; Ha, Y.; Ahn, J.; Facchetti, A.; Marks, T. J.; Rogers, J. A. Self-Assembled Nanodielectrics and Silicon Nanomembranes for Low Voltage, Flexible Transistors, and Logic Gates on Plastic Substrates. *Appl. Phys. Lett.* **2009,** *95*, 183504/1–183504/3.

(10) Hur, S.; Yoon, M.; Gaur, A.; Shim, M.; Facchetti, A.; Marks, T. J.; Rogers, J. A. Organic Nanodielectrics for Low Voltage Carbon Nanotube Thin Film Transistors and Complementary Logic Gates. *J. Am. Chem. Soc.* **2005,** *127*, 13808–13809.

(11) Ju, S.; Kim, S.; Mohammadi, S.; Janes, D. B.; Ha, Y.; Facchetti, A.; Marks, T. J. Interface Studies of ZnO Nanowire Transistors Using Low-Frequency Noise and Temperature-Dependent *I*–*V* Measurements. *Appl. Phys. Lett.* **2008,** *92*, 022104/1–022104/3.

(12) Chen, P.; Shen, G.; Chen, H.; Ha, Y.; Wu, C.; Sukcharoenchoke, S.; Fu, Y.; Liu, J.; Facchetti, A.; Marks, T. J.; et al. High-Performance Single-Crystalline Arsenic-Doped Indium Oxide Nanowires for Transparent Thin-Film Transistors and Active Matrix Organic Light-Emitting Diode Displays. *ACS Nano* **2009,** *3*, 3383–3390.

(13) Kim, H. S.; Byrne, P. D.; Facchetti, A.; Marks, T. J. High Performance Solution-Processed Indium Oxide Thin-Film Transistors. *J. Am. Chem. Soc.* **2008,** *130*, 12580–12581.

(14) Ju, S.; Lee, K.; Janes, D. B.; Yoon, M.; Facchetti, A.; Marks, T. J. Low Operating Voltage Single ZnO Nanowire Field-Effect Transistors Enabled by Self-Assembled Organic Gate Nanodielectrics. *Nano Lett.* **2005,** *5*, 2281–2286.

(15) Ju, S.; Lee, K.; Yoon, M.; Facchetti, A.; Marks, T. J.; Janes, D. B. High Performance ZnO Nanowire Field Effect Transistors with Organic Gate Nanodielectrics: Effects of Metal Contacts and Ozone Treatment. *Nanotechnology* **2007,** *18*, 155201/1–155201/7.

(16) For a general overview of Weibull analysis, the reader is directed to refs 22−24.

(17) Weibull, W. J. A Statistical Distribution Function of Wide Applicability. *Appl. Mech.* **1951,** *18*, 293–297.

(18) Snyder, E.; Suehle, J. In *Integrated Reliability Workshop Final Report*, Lake Tahoe, CA, October 18−23, 1999; IEEE International: Los Alamitos, CA, 1999.

(19) Kauerauf, T.; Degraeve, R.; Cartier, E.; Soens, C.; Groeseneken, G. Low Weibull Slope of Breakdown Distributions in High-*k* Layers. *IEEE Electr. Device L* **2002,** *23*, 215–217.

(20) Kim, Y. H.; Onishi, K.; Kang, C. S.; Cho, H.; Choi, R.; Krishnan, S.; Akbar, M.; Lee, J. C. Thickness Dependence of Weibull Slopes of HfO_2 Gate Dielectrics. *IEEE Electron Device Lett.* **2003,** *24*, 40–42.

(21) Ju, S.; Janes, D. B.; Lu, G.; Facchetti, A.; Marks, T. J. Effects of Bias Stress on ZnO Nanowire Field-Effect Transistors Fabricated with Organic Gate Nanodielectrics. *Appl. Phys. Lett.* **2006,** *89*, 193506/1–193506/3.

(22) Dodson, B. *Weibull Analysis*; ASQC Quality Press: Milwaukee, WI, 1994.

(23) Wu, E.; Vollertsen, R. On the Weibull Shape Factor of Intrinsic Breakdown of Dielectric Films and its Accurate Experimental

Determination. Part I: Theory, Methodology, Experimental Techniques. *IEEE Trans. Electron Devices* **2002,** *49*, 2131–2140.
(24) Dissado, L. A. Weibull Statistics in Dielectric Breakdown; Theoretical Basis, Applications and Implications. *J. Phys. D.: Appl. Phys.* **1990,** *23*, 1582–1591.
(25) Wu, E.; Sune, J.; Lai, W. On the Weibull Shape Factor of Intrinsic Breakdown of Dielectric Films and Its Accurate Experimental Determination. Part II: Experimental Results and the Effects of Stress Conditions. *IEEE Trans. Electron Devices* **2002,** *49*, 2141–2150.
(26) Dissado, L.; Fothergill, J.; Wolfe, S.; Hill, R. Weibull Statistics in Dielectric Breakdown; Theoretical Basis, Applications and Implications. *IEEE Trans. Electr. Insul.* **1984,** *EI-19*, 227–233.
(27) Hill, R. M.; Dissado, L. A. Theoretical Basis for the Statistics of Dielectric Breakdown. *J. Phys. C. Solid State* **1983,** *16*, 2145–2156.
(28) Costa, U.; Freire, V.; Malacarne, L.; Mendes, R.; Picoli, S., Jr.; de Vasconcelos, E.; da Silva, E., Jr. An Improved Description of the Dielectric Breakdown in Oxides Based on a Generalized Weibull Distribution. *Physica A* **2006,** *361*, 209–215.
(29) Picoli, S.; Mendes, R. S.; Malacarne, L. C. q-Exponential, Weibull, and q-Weibull Distributions: An Empirical Analysis. *Physica A* **2003,** *324*, 678–688.
(30) Jose, K. K.; Naik, S. On the q-Weibull Distribution and Its Applications. *Commun. Stat. Theory* **2009,** *38*, 912–926.

DOI: 10.1021/jz101325r | *J. Phys. Chem. Lett.* **2010,** *1*, 3292–3297